Acidic pH-responsive polymer nanoparticles as TLR7/8 agonist delivery platform for cancer immunotherapy

Journal:	*Nanoscale*
Manuscript ID	NR-ART-09-2018-007201.R1
Article Type:	Paper
Date Submitted by the Author:	07-Oct-2018
Complete List of Authors:	Kim, Hyunjoon; University of Minnesota, Department of Pharmaceutics Sehgal, Drishti; University of Minnesota, Department of Pharmaceutics Kucaba, Tamara; University of Minnesota, Department of Urology Ferguson, DM; University of Minnesota, Department of Medicinal Chemistry Griffith, Thomas; University of Minnesota, Department of Urology Panyam, Jayanth; University of Minnesota, Department of Pharmaceutics

Acidic pH-responsive polymer nanoparticles as TLR7/8 agonist delivery platform for cancer immunotherapy

Authors: Hyunjoon Kim[a], Drishti Sehgal[a], Tamara A. Kucaba[b], David M. Ferguson[c], Thomas S. Griffith[b,d,e,f], Jayanth Panyam[a,d]*

Affiliations:

[a]Department of Pharmaceutics, University of Minnesota, Minneapolis, MN, 55455.

[b]Department of Urology, University of Minnesota, Minneapolis, MN, 55455.

[c]Department of Medicinal Chemistry, University of Minnesota, Minneapolis, MN, 55455.

[d]Masonic Cancer Center, University of Minnesota, Minneapolis, MN, 55455.

[e]Center for Immunology, University of Minnesota, Minneapolis, MN, 55455.

[f]Microbiology, Immunology, and Cancer Biology Graduate Program, University of Minnesota, Minneapolis, MN, 55455.

* Corresponding author. Department of Pharmaceutics, College of Pharmacy, University of Minnesota, Minneapolis, MN 55455, USA. E-mail address: jpanyam@umn.edu (J. Panyam).

Keywords: Immunotherapy, Nanoparticles, TLR7/8 agonist, pH-responsive drug delivery

Abstract

Synthetic imidazoquinoline-based toll-like receptor (TLR) 7/8 bi-specific agonists are promising vaccine adjuvants that can induce maturation of dendritic cells (DCs) and activate them to secrete pro-inflammatory cytokines. However, *in vivo* efficacy of these small molecule agonists is often hampered by their fast clearance from the injection site, limiting their use to topical treatments. In this study, we investigated the use of acidic pH-responsive poly(lactide-co-glycolide) (PLGA) nanoparticles for endo-lysosome specific release of 522, a novel TLR7/8 agonist. Bicarbonate salt was incorporated in the new formulation to generate carbon dioxide ($CO_{2)}$ gas in acidic pH, which can disrupt the polymer shell to rapidly release the payload. Compared to conventional PLGA nanoparticles, the pH responsive formulation resulted in 33-fold higher loading of 522. The new formulation demonstrated acid-responsive CO_2 gas generation and drug release. The acid-responsive formulation increased the *in vitro* expression of co-stimulatory molecules on DCs and improved antigen-presentation via MHC I, both of which are essential for CD8 T cell priming. *In vivo* studies showed that pH-responsive formulation elicited stronger antigen-specific CD8 T cell and natural killer (NK) cell responses than conventional PLGA nanoparticles, resulting in enhanced anticancer efficacy in a murine melanoma tumor model. Our results suggest that acidic-pH responsive, gas-generating nanoparticles is an efficient TLR7/8 agonist delivery platform for cancer immunotherapy.

Introduction

Imidazoquinoline-based synthetic toll-like receptor (TLR) 7/8 agonists are promising vaccine adjuvants for cancer immunotherapy [1]. TLR7/8 ligation triggers MyD88-dependent signaling in dendritic cells (DC), resulting in the production of pro-inflammatory cytokines and co-stimulatory molecule expression [2]. DC activation leads to expansion of activated natural killer (NK) cells and antigen (Ag)-specific CD8 T cells, both of which can kill malignant tumor cells [3]. Current vaccine designs seek to deliver TLR agonists to DCs present in the skin and/or draining lymph nodes [4]. However, small molecules are not retained in the skin for an extended duration because of rapid clearance from the well-vascularized dermal layers. This can result in undesirable systemic immune response [5]. Further, following uptake by DCs, the agonist molecules have to distribute into endo-lysosomes to activate TLR 7/8 [6]. Thus, endo-lysosomal specific delivery of the agonists to DCs present in the dermal layers and lymph nodes can result in efficient TLR7/8 ligation and superior anticancer immune response.

We previously reported the use of poly(D,L-lactide-co-glycolide) (PLGA) nanoparticles for the delivery of a novel TLR7/8 agonist (termed '522') [7]. These nanoparticles (referred to as '522NP') traffic to draining lymph nodes after subcutaneous (S.C.) injection and potently activate DCs. When combined with a peptide or whole tumor cell lysate-based Ag, 522NP immunization significantly increased the number of Ag-specific effector CD8 T cells. Moreover, this vaccination modality enhanced the prophylactic and therapeutic anticancer efficacy in murine tumor models. Yet, these nanoparticles were limited by low encapsulation efficiency (which limited the dose of 522 that could be used) and non-specific agonist release.

In this study, we investigated the use of acidic pH responsive PLGA nanoparticles to both increase agonist encapsulation and improve endo-lysosome (pH 4-6)-specific agonist release. We hypothesized the higher dose and acidic-pH responsive release of 522 would result in

stronger activation of DCs and elicit robust CD8 T cell response for enhanced cancer immunotherapy. We adapted the use of bicarbonate salt, which generates carbon dioxide (CO_2) gas in acidic pH, to incorporate pH responsiveness. Thus, NPs encapsulating both 522 and sodium bicarbonate were expected to generate CO_2 gas in the acidic pH of the endo-lysosomes and mechanically disrupt the polymer matrix, resulting in a burst release of the encapsulated 522 in endo/lysosomes. In our study, co-incorporation of sodium bicarbonate resulted in significantly increased encapsulation of 522 and acidic pH responsive 522 release. Our data further suggest this new formulation elicits a much stronger anti-cancer immune response than conventional PLGA NPs.

Experimental

Materials

Poly(lactide-*co*-glycolide) (PLGA) (50:50 lactide-glycolide ratio; 0.55-0.75 dl/g inherent viscosity) was purchased from Lactel (Birmingham, AL). TLR 7/8 agonist (termed '522') was synthesized and characterized as previously reported [8,9]. Albumin from chicken egg white (ovalbumin, OVA), polyvinyl alcohol (PVA), 6-coumarin, ammonium acetate and dimethyl sulfoxide (DMSO) were purchased from Sigma-Aldrich (St Louis, MO). Sodium bicarbonate, chloroform, acetonitrile, fluorescein conjugated ovalbumin, Foxp3 transcription factor staining buffer kit were purchased from Fisher Scientific (Rockford, IL). Fluorophore-labeled monoclonal antibodies for flow cytometry were purchased from Biolegend (San Diego, CA) (CD3, CD8, CD11c, CD80, CD49b, CD69, IFN-γ), eBioscience (San Diego, CA) (CD4, CD44, CD40, CD86) and Tonbo Biosciences (San Diego, CA) [I-A/I-E(MHC II)].

Animals and cell line

All animal experiment protocols were reviewed and approved by Institutional Animal Care and Use Committee (IACUC) of the University of Minnesota, an accredited program through the Association for Assessment and Accreditation of Laboratory Animal Care (AAALAC). All animal studies were conducted according to the approved protocol and researchers followed the ethical, legal and safety regulations of NIH guidelines of animal care. Immunocompetent C57BL/6 mice (7-8 weeks, female) were purchased from Charles River (Wilmington, MA) and housed under specific pathogen free (SPF) units in Research Animal Resources at the University of Minnesota.

B16F10-OVA, a murine melanoma cell line which expresses ovalbumin, was provided by Dr. Brandon Burbach (University of Minnesota). B16F10-OVA was cultured in RPMI 1640 medium supplemented with 10% fetal bovine serum, 100 μg/mL streptomycin, 100 U/mL penicillin (hereafter referred to as complete RPMI) and 5 μg/mL G-418 Disulfate (Research products international, Mt Prospect, IL).

Fabrication of nanoparticles

522NP formulation was prepared as previously reported [7], using 3 mg 522 and 44 mg PLGA. Acidic pH-responsive nanoparticle formulation of 522 (hereafter referred to as '522GGNP') were formulated using a variation of the water-in-oil-in-water (w/o/w) double-emulsion solvent evaporation technique. For the primary w/o emulsion, the aqueous phase was prepared by dissolving 2.5 mg of sodium bicarbonate in 500 μl of 1% w/v PVA in endotoxin-free distilled water (D.I. water). This aqueous phase was transferred to the oil phase, which consisted of 44 mg PLGA and 3 mg 522 dissolved in 2 ml chloroform. This mixture was

sonicated using probe sonicator (Sonicator XL, Misonix, Melville, NY) for 1 min to form w/o emulsion. This primary emulsion was then added to 8 ml of 2% PVA and sonicated for 5 min to form secondary w/o/w emulsion. The final emulsion was stirred for ~18 h, followed by 1 h in a desiccator under vacuum to evaporate chloroform. Nanoparticle dispersion formed was washed by centrifugation (Optima XPN-80 Ultracentrifuge, Beckman Coulter Inc., Fullerton, CA) (35,000 RPM, 35 min) and reconstitution with D.I. water three times. After final wash, nanoparticles were resuspended in D.I. water and lyophilized (Labconco FreeZone 4.5, Kansas City, MO). Nanoparticles were stored at -20°C until use.

Characterization of nanoparticles

To determine size and zeta potential of the nanoparticles, ~1 mg of nanoparticles were dispersed in D.I. water and sonicated for 30 sec and subjected to dynamic light scattering (DLS) analysis (Delsa^{TM} Nano C, Beckman Coulter Inc.). Nanoparticles were also imaged using a cryo-transmission electron microscope (TEM) (FEI Tecnai G2 F30) as described previously [10].

The amount of 522 encapsulated into the nanoparticles was quantified using high-performance liquid chromatography (HPLC; Beckman Coulter) as previously reported [7]. The amount of sodium bicarbonate encapsulated into the nanoparticles was measured by quantifying sodium ion using inductively coupled plasma optical emission spectrometry (ICP-OES) (Thermo Scientific iCAP 6000 Series). Briefly, a mixture of nitric acid and hydrochloric acid (3:1 molar ratio) was added to 1 mg of nanoparticles in a glass vial. Glass vial was heated to 90°C in an oil bath for 5 h to fully dissolve nanoparticles. Mixture was then cooled and diluted with D.I. water for ICP-EOS analysis.

Cytotoxicity of nanoparticles

Splenocytes from C57BL/6 mice were used to measure cytotoxicity of nanoparticles. A single cell suspension of splenocytes was prepared using an established protocol [11]. Briefly, spleens were mechanically homogenized using gentleMACS Dissociator (Miltenyi BioTeck Inc., Auburn, CA). The cell suspension was washed with HBSS and digested in HBSS supplemented with 0.15 mg/ml DNAse I (Sigma) and 0.56 Wuensch units/ml Liberase Blendzyme 3 (Roche, Branford, CT). After 30 min, red blood cells (RBCs) were removed by incubating the cell suspension with lysis buffer (Pharm Lyse, BD Bioscience, San Jose, CA) with for 5 min. Cells were then washed with PBS and suspended in HBSS until further use. To evaluate cytotoxicity of nanoparticles, mouse splenocytes (2 x 10^4 cells/well) were incubated with 522GGNP (15.6~250 μg/ml) in a 96-well plate. After 48 h incubation period, supernatants were collected and cytotoxicity was determined according to the manufacturer's protocol (LDH Cytotoxicity Assay Kit, Thermo).

TLR7 and 8 reporter cell assay

Human TLR-specific reporter cell assays were performed as previously reported [8]. Reporter cells (HEK-Blue™-hTLR7 and 8, InvivoGen, San Diego, CA) (40,000 cells per well) were seeded in 96-well cell culture plate, and soluble form of 522 in DMSO (referred to as 'Free522') (30 μM) or 522GGNP (522 equivalent to 30 μM) were added to the wells. After 24 h, supernatants were collected for measuring TLR-specific activity according to manufacturer's protocol.

***In vitro* release kinetics**

Release of 522 from 522GGNPs was determined in acidic (5.5, 6.5) and neutral pH (7.4) buffers. Release buffer was added to 1 mg of nanoparticles in 2 ml plastic tubes. Sample tubes were incubated in a water bath shaker at 37°C (100 RPM). At pre-determined time points, samples were centrifuged and 0.5 ml of the supernatant was collected. Sample tubes were refilled with fresh 0.5 ml buffer to maintain a constant volume. Collected samples were lyophilized and agonist was extracted with methanol. Amount of agonist released at each time point was analyzed using HPLC.

Generation of CO_2 bubbles was tested as previously described [12]. Briefly, 10 ml of buffer solution (pH 5.5 or 7.4) was added to ~6 mg of nanoparticles in a 15-ml plastic tube. The CO_2 bubbles generated were visualized using an ultrasound imaging system (Vevo2100, Visualsonics) equipped with a 21 MHz transducer. Intensity of bubbles were measured by quantifying white values in ultrasound images using ImageJ software. Sodium bicarbonate (50 mg) and 522NPs (6 mg) were used as positive and negative controls, respectively.

Culture of bone marrow-derived dendritic cells (BMDCs)

BMDCs were prepared as described previously [7]. Briefly, bone marrow precursor cells were collected from tibias and femurs from C57BL/6 mice. Cells were filtered with a 70 micron nylon mesh and red blood cells were removed using lysis buffer to obtain single cell suspension. Cells were seeded in petri dish and incubated with complete RPMI media, supplemented with 20 ng/mL granulocyte-macrophage colony-stimulating factor (GM-CSF) (PeproTech, Rocky Hill, NJ), 10 ng/mL IL-4 and 50 μM 2-mercaptoethanol (Sigma) for 6 d to generate immature BMDCs.

Uptake of nanoparticles in BMDCs

To label and track nanoparticles, 6-coumarin, a hydrophobic fluorescent dye, was co-encapsulated in 522GGNPs by adding 300 μg of 6-coumarin to the organic phase during 522GGNP fabrication [13]. For *in vitro* cell uptake study, BMDCs were seeded in a 24-well culture plate (10^6/well), and then incubated with NPs (0.2 mg/ml) for 2 h. Cells were collected, washed with PBS, and stained with anti-CD11c mAb. Uptake of NPs by BMDCs was examined by monitoring 6-coumarin-associated fluorescence intensity by flow cytometry (BD LSR II). Flow cytometry data were analyzed using FlowJo software (TreeStar Inc., Ashland, OR).

Intracellular distribution of NPs was imaged by confocal laser scanning microscopy (Olympus FluoView FV1000 BX2 Upright Confocal). Glass-bottomed petri dishes (35 mm, MatTek) were coated with poly-L-lysine solution (Sigma) for 30 min. After 30 min, the poly-L-lysine solution was removed and petri dishes were rinsed with D.I. water twice. Dishes were dried in a laminar flow hood for 2 h, and BMDCs ($3x10^5$/dish) were added. After 24 h, BMDCs were incubated with NPs (0.2 mg/ml) for 4 h, and rinsed with PBS. Cells were counterstained with LysoTracker® Red DND-99 (Thermo Scientific) and imaged without fixation.

***In vitro* BMDC activation**

BMDCs (10^6/well) were added to a 24-well cell culture plate. Following attachment, BMDCs were treated with OVA (20 μg) alone or OVA combined with 522NPs (100 μg/ml, equivalent to 120 ng/ml of 522) or 522GGNPs (100 μg /ml, equivalent to 4 μg/ml of 522) for 24 h. Expression of co-stimulatory molecules (CD40, CD80 and CD86) and MHC II on BMDCs was measured by flow cytometry.

In vitro BMDC antigen uptake and presentation

Antigen uptake by BMDCs was measured by flow cytometry. A solution of fluorescein conjugated OVA (OVA-FITC, Thermo) in PBS (10 μg/ml) was added to BMDCs ($1x10^6$/well). Subsequently, cells were incubated with 0.1 mg of 522NP or 522GGNP for 6 h. Cells were then washed with PBS and stained with anti-CD11c mAb. FITC associated fluorescence intensity was measured in $CD11c^+$ cells by flow cytometry. To examine antigen presentation by BMDCs, the above experiment was repeated by incubating unlabeled OVA (20 μg) with BMDCs for 24 h. After 24 h, BMDCs were harvested and stained with anti-CD11c antibody and anti-$OVA_{257-264}$ (SIINFEKL) peptide bound to H-$2K^b$ (clone 25-D1.16; eBioscience) antibody and analyzed by flow cytometry.

Immunization protocol

Vaccine doses were prepared by combining OVA (100 μg) with 1.5 mg of 522NPs (equivalent to 1.8 μg of 522) or 522GGNPs (equivalent to 60 μg of 522) in 200 μl of sterile PBS. Each dose was injected s.c. to the left and right thighs (100 μl each). Mice were dosed once every day for five consecutive days.

In vivo T cell and NK cell activation assays

Immunocompetent C57BL/6 mice were immunized daily as described above for 5 d (d 1~5). On d 10, mice received 100 μg of $OVA_{257-264}$ peptide via tail vein injection and euthanized after 4 h. Spleen was collected and a single cell suspension of splenocytes was prepared as described above and stained with anti-CD3, anti-CD4, anti-CD8, anti-CD44, anti-CD49b and anti- IFN-γ antibodies as well as with $OVA_{257-264}$:H-$2K^b$ Tetramer-APC. Intracellular staining of

IFN-γ was conducted according to the manufacturer's protocol (Foxp3/Transcription Factor Staining Buffer Set, eBioscience). Number of cells per spleen was calculated by using counting beads (eBioscience) in flow cytometry analysis.

Tumor challenge

B16F10-OVA cells (5 x 10^5) were suspended in 100 µl PBS and inoculated s.c. in the abdominal region near the right thigh of C57BL/6 mice. Tumor volume was measured as previously described [7]. Once the tumor volume reached 100 mm^3, mice were immunized as described above. Mice that grew tumors >1500 mm^3 and/or developed ulcerations in the tumor were euthanized.

Statistical analyses

Results were shown as either mean ± standard deviation (SD) or mean ± standard error of the mean (SEM). One-way analysis of variance (ANOVA) with *post hoc* Tukey test was used to determine the statistical significance of the observed differences between the treatment groups, unless otherwise noted. A *p*-value ≤ 0.05 was considered statistically significant; *p*-values were indicated using the following scheme: *$p \leq 0.05$, **$p \leq 0.01$, ***$p \leq 0.001$, n.s = not significant ($p > 0.05$). Data was analyzed using GraphPad Prism 7 software.

Results

Physicochemical characterization and TLR 7/8 specific activity by NPs

522GGNPs were similar to 522NPs in physicochemical characteristics. 522GGNPs appeared as discrete spheres and without apparent aggregation when imaged by cryo-TEM

(Figure 1A). Average diameter of 522GGNP measured by DLS was 202 ± 3 nm, which was similar to that of 522NPs (210 ± 2 nm) **(Table 1)**. 522GGNPs were negatively charged, with an average zeta-potential of -16.5 ± 2 mV, which was comparable to that of 522NPs (-22.6 ± 1.9 mV). However, 522 encapsulation was 33-fold higher in 522GGNPs (40 μg/mg of NP) than in 522NP (1.2 μg/mg of NP). Loading of sodium bicarbonate in 522GGNP was confirmed using ICP-EOS and was 8.8 μg/mg of NP.

522GGNPs caused negligible cytotoxicity against mouse splenocytes **(Figure 1B)**, which is consistent to the previous studies reporting minimal cytotoxicity of PLGA nanoparticles [14,15]. We then investigated whether 522GGNPs can specifically activate TLR7 and TLR8 in TLR reporter cells. As shown at **Figure 1C**, 522 maintained its TLR7 and 8 activity after encapsulation in NPs.

(A)

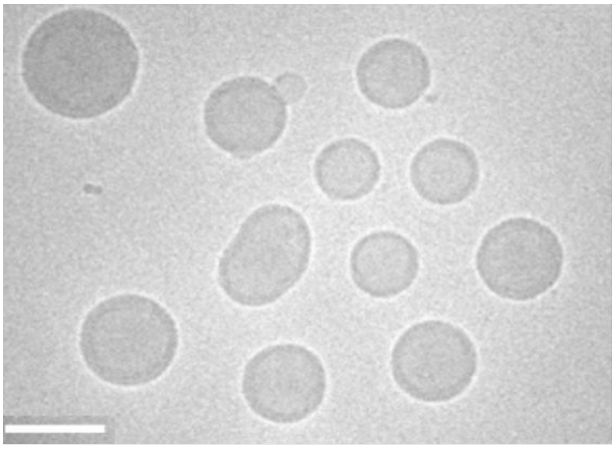

(B)

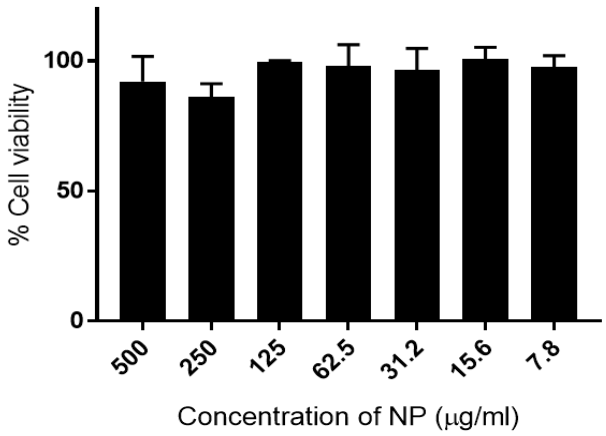

(C)

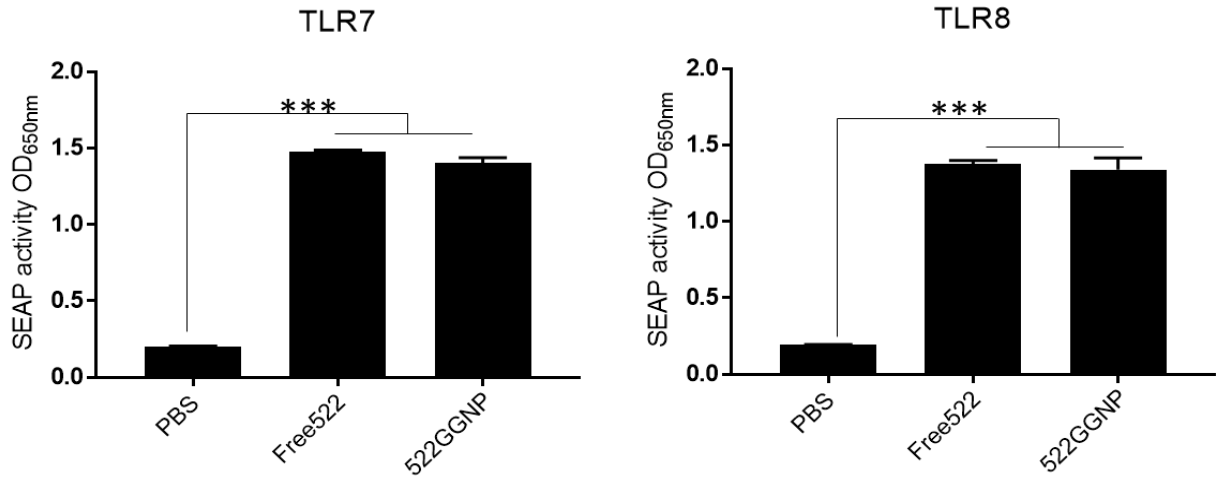

Figure 1. 522GGNP *in vitro* efficacy

(A) A representative cryo-TEM image of 522GGNPs. Scale bar, 100 nm. **(B)** Cytotoxicity of 522GGNP against mouse splenocytes. Treatments were incubated with mouse splenocytes for 48 h and cytotoxicity was measured by LDH assay. Results are reported as mean ± SD, n=4. **(C)** Human TLR7 or TLR8 specific reporter cells were incubated with DMEM, Free522 and 522GGNP for 24 h. TLR specific activation by treatments was measured by SEAP activity at OD_{650}. Results are reported as mean ± SD, n=4, ***p<0.001, One-way ANOVA.

	522NP	522GGNP
Particle size (nm)	210 ± 2	202 ± 3
Zeta-potential (mV)	-22.6 ± 1.9	-16.5 ± 2
Polydispersity index	0.12 ± 0.02	0.14 ± 0.01
Loading amount of 522 (μg/mg NP)	1.2 ± 0.1	40 ± 1.8
Loading efficiency (%)	1.8 ± 0.1	60 ± 2.7

Amount of $NaHCO_3$ (μg/mg NP)	-	8.8 ± 2.9

Table 1. Physiochemical characterization of 522NPs and 522GGNPs

Particle size, zeta-potential and polydispersity index of NPs were measured by DLS. Amount of 522 loaded in nanoparticles was quantified using HPLC. Amount of sodium bicarbonate in the 522GGNPs was measured using ICP-EOS. Results are reported as mean ± SD, n=3.

***In vitro* release kinetics and gas-generation by NPs**

522GGNPs showed acidic pH-responsive release kinetics **(Figure 2A)**. In the first hour, 522GGNPs released ~90% and ~72% of encapsulated 522 in pH 5.5 and 6.5 buffers. In the neutral pH, however, 522GGNPs released only ~23% of the encapsulated 522 in the first 1 h, followed by slower release (~85%) over the next 48 h. We then monitored CO_2 generation by 522GGNPs using ultrasound imaging **(Figure 2B)**. In pH 5.5, sodium bicarbonate (positive control) generated large number of CO_2 bubbles. Generation of CO_2 bubbles was significantly lower but still detectable in pH 7.4. For 522NP, we detected negligible CO_2 generation at either pH. 522GGNPs demonstrated significant CO_2 generation in acidic pH but not in pH 7.4 **(Figure 2C)**. These results provide direct evidence that 522GGNP generate CO_2 bubbles in acidic pH.

(A)

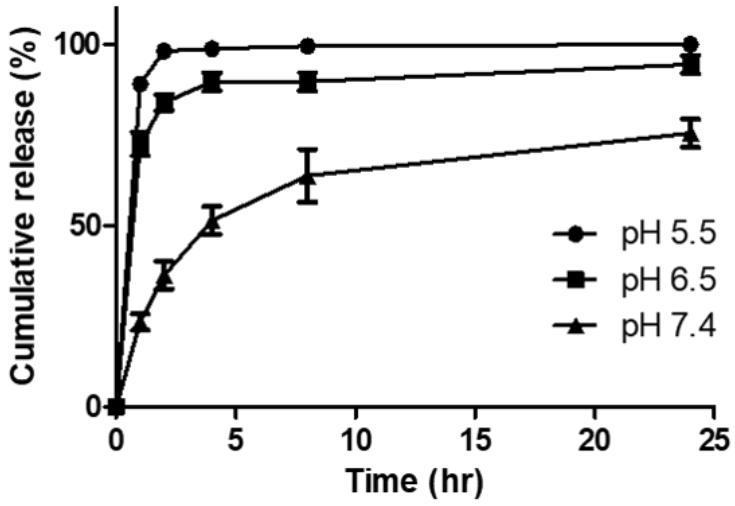
Cumulative release (%)
100
50
0
0
5
10
15
20
25
Time (hr)
pH 5.5
pH 6.5
pH 7.4

(B)

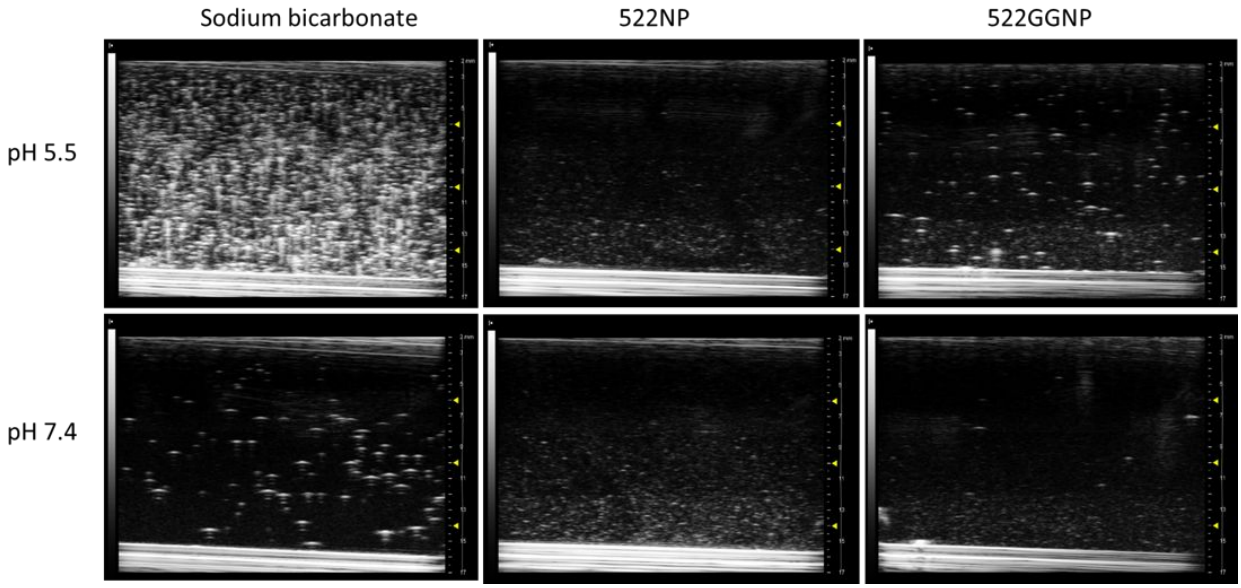
Sodium bicarbonate
522NP
522GGNP
pH 5.5
pH 7.4

(C)

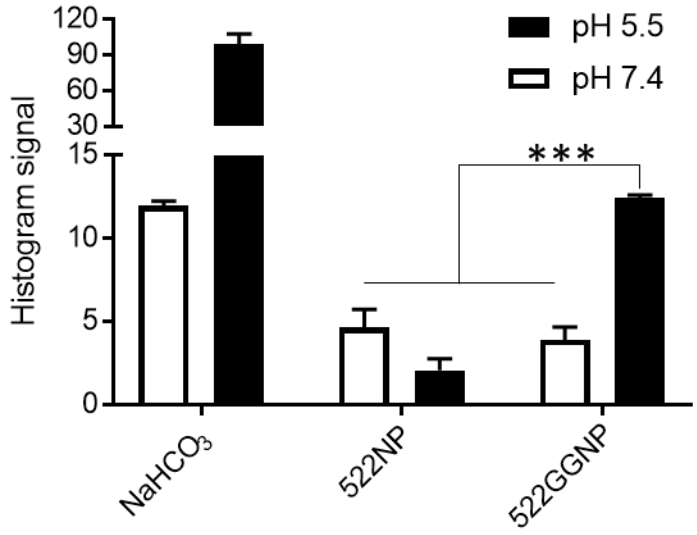

Figure 2. 522GGNP *in vitro* release kinetics and gas generation profiles

(A) Cumulative release of 522 from 522GGNP was measured in pH 5.5, 6.5 and 7.4. Results are reported as mean ± SD, n=3. **(B)** Gas generation from sodium bicarbonate and nanoparticles was visualized by ultrasound imaging. Representative ultrasound images at pH 5.5 and 7.4 are shown. (C) Generated gas was quantified by measuring histogram intensity of white signals. Results are reported as mean ± SD, n=4. ***$p<0.001$, One-way ANOVA.

NP uptake by BMDCs

Uptake of 522GGNPs by DCs and their trafficking to the endo/lysosomal compartment is critical for efficient TLR7/8 activation [16]. As shown in **Figure 3A**, there was a clear shift in fluorescence intensity of BMDCs treated with NPs, which indicates that BMDCs were associated with the labeled NPs. To further investigate the internalization and intracellular trafficking, we imaged BMDCs using confocal laser microscopy **(Figure 3B)**. Consistent with our previous study, 6-coumarin labeled 522NPs (C6NPs) (green fluorescence), were located in both the

cytosol and endo/lysosome (stained with red fluoresnce). However, we observed greater presence of merged signal (yellow fluorescence) from 6-coumarin labeled 522GGNP (C6GGNP) treated BMDCs than those treated with C6NPs. These results suggest that GGNP formulation can enhance the endo/lysosomal delivery of 522.

(A)

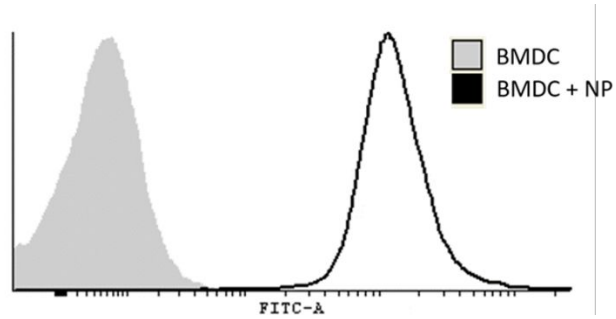

(B)

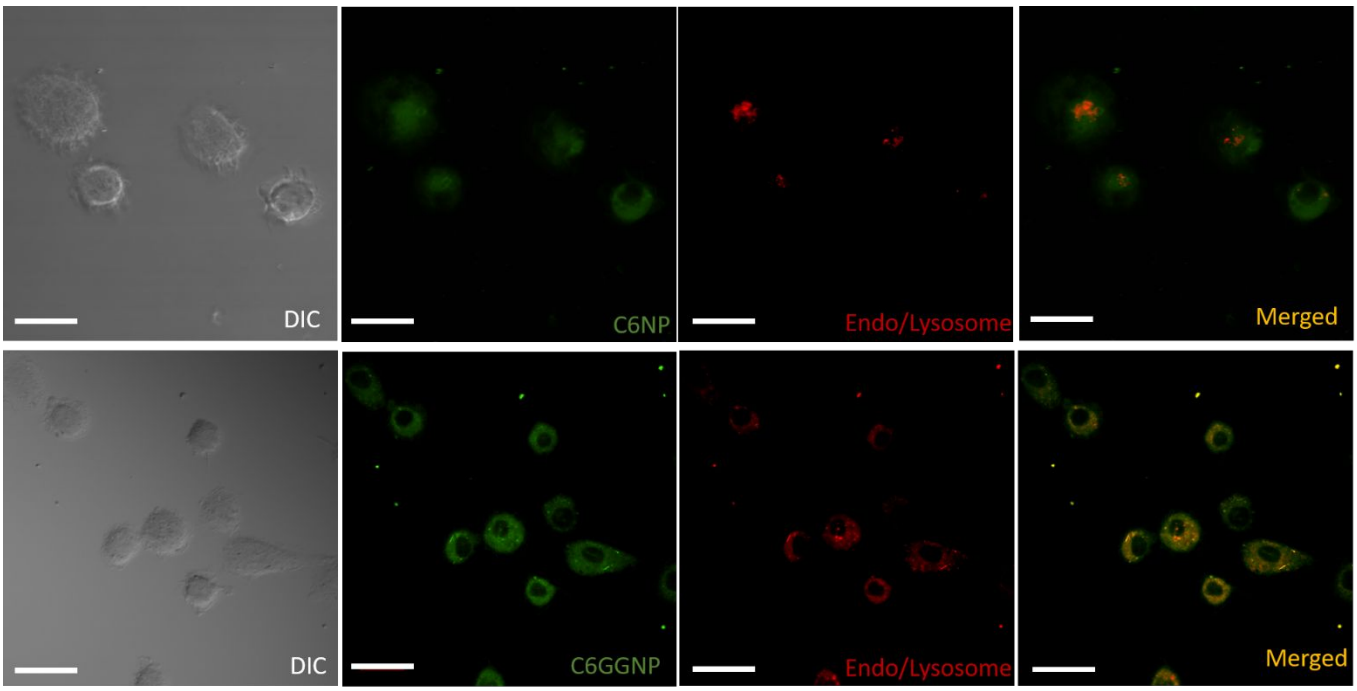

Figure 3. NP uptake by BMDC

(A) 6-coumarin labeled 522GGNPs(C6GGNP) and 522NPs (C6NP) were incubated with BMDCs ($CD11c^+$) for 2 h, and change in fluorescence intensity of BMDCs was measured by flow cytometry. Representative histograms of fluorescence intensity are shown. **(B)** A representative confocal image of BMDCs after incubation with 522GGNPs is shown. Green: nanoparticles, red: endo/lysosomes, yellow: merged signal of nanoparticle and endo/lysosomes. Scale bar, 20 μm.

BMDC activation

To elicit CD8 T cell response, DC expression of co-stimulatory molecules CD40, CD80 and CD86 is essential [17]. Therefore, we measured the extent of DC activation in the presence of 522GGNPs by measuring co-stimulatory molecule expression. OVA was used as a model antigen in these studies. As expected, OVA alone had negligible effect on DC activation. CD40 expression increased from 5% for untreated to 89% for OVA+522GGNP treatment, while 11% and 69% of the BMDC expressed CD40 when treated with OVA only and OVA+522NP, respectively **(Figure 4A)**. OVA+522GGNP treatment also increased the frequency of BMDC expressing CD86 to 71%, while OVA only and OVA+522NP treatment resulted in 18% and 33% of the BMDC expressing CD86, respectively. CD80 also showed similar trend, where OVA+522GGNP treatment induced 66% of the cells to expression CD80, while OVA only and OVA+522NP treatments resulted in 16% and 23%, respectively. In addition to co-stimulatory molecule upregulation, OVA+522GGNP increased MHC II expression on DCs by 54%, while OVA only and OVA+522NP treated DCs had 29% and 34% expression, respectively **(Figure 4B)**. These data show 522GGNPs results in enhanced DC activation compared to 522NPs.

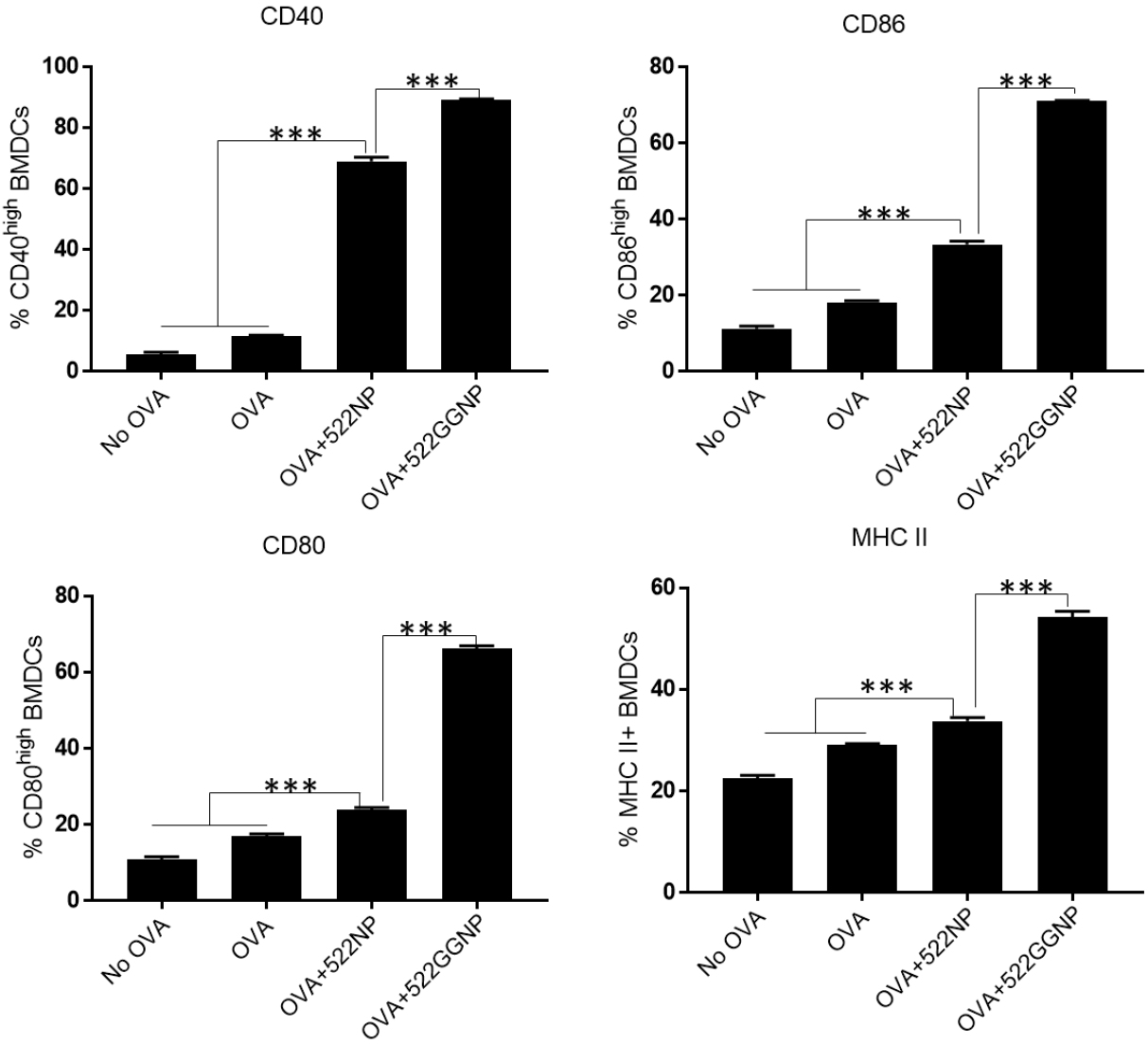

Figure 4. BMDC activation

Flow cytometry analysis of CD40, CD80, CD86 and MHC II expression on BMDCs after 48 h incubation with treatments. Results are reported as mean ± SD, n=4, ***p<0.001, One-way ANOVA.

Antigen uptake and presentation

We also investigated the other key feature of successful DC activation: Ag uptake and presentation via MHC I [18]. We determined the effect of co-incubation with 522GGNPs on Ag uptake by DCs using fluorescently-labeled OVA. After 1 h incubation, a significant increase in DC fluorescence intensity was observed **(Figure 5A,B),** suggesting internalization of OVA-FITC. There was a statistically significant increase in OVA uptake when DCs were co-treated with 522NP, and the highest increase was detected when DCs were co-treated with 522GGNPs. Uptake of Ag does not necessarily leads to Ag presentation by DCs [19]. Therefore, we measured $OVA_{257-264}$ (SIINFEKL) peptide:MHC I complex on DCs, [20]. Compared to Ag uptake, OVA+522GGNP treated BMDCs showed 4- and 2-fold higher expression of $OVA_{257-264}$ (SIINFEKL) peptide:MHC I complex compared to the OVA only and OVA+522NP incubated BMDCs, respectively **(Figure 5C)**. These data suggest that 522GGNP not only enhance the Ag uptake of DCs, but also potentiates Ag-presentation via MHC I, that results in expansion of Ag-specific cytotoxic CD8 T cells.

(A)

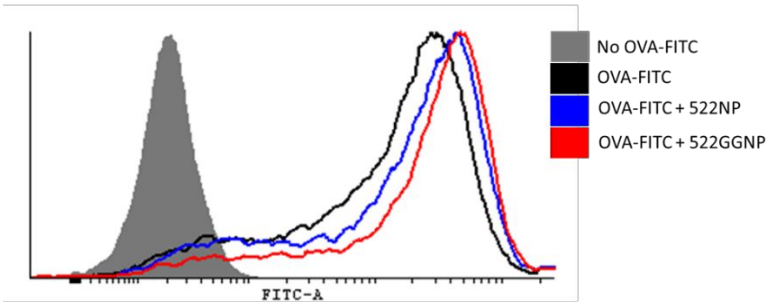

(B)

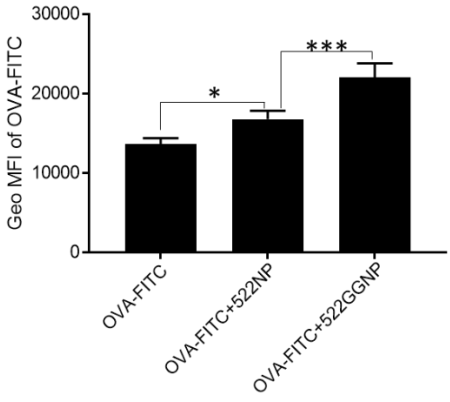

(C)

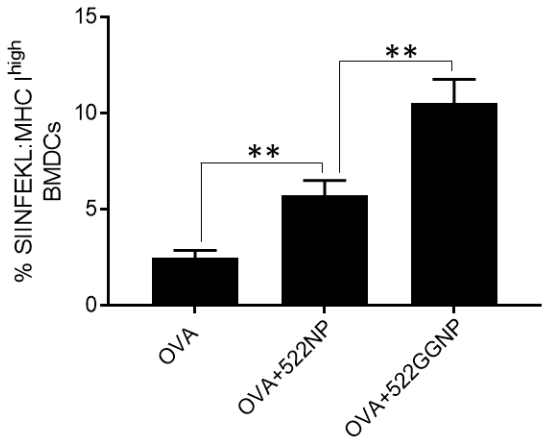

Figure 5. Antigen uptake and presentation via MHC I

(A,B) FITC labeled ovalbumin (OVA-FITC) and treatments were incubated with BMDCs for 6 h. **(A)** A representative histogram showing fluorescence intensity of BMDCs is shown. **(B)** FITC fluorescence was quantified as geometric mean fluorescence intensity. Results are reported as mean ± SD, n=4, *p<0.05, ***p<0.001, One-way ANOVA. (C) BMDCs were incubated with OVA and/or NPs for 48 h. BMDCs expressing $OVA_{257-264}$ (SIINFEKL) peptide bound to H-$2K^b$ (MHC I) were analyzed by flow cytometry. Results are reported as mean ± SD, n=3, **p<0.01, One-way ANOVA.

***In vivo* T cell assay**

We next examined the extent of T cell response after immunizing immunocompetent mice. We first measured CD4 T cells, which enhance CD8 T cell activation by secreting IFN-ɣ [21,22]. The number of IFN-ɣ$^{+}$ CD4 T cells increased 2-fold when mice were immunized with OVA+522GGNP compared to untreated and OVA only groups **(Figure 6A)**. OVA+522NP treated mice also showed increased IFN-ɣ$^{+}$ CD4 T cells compared to the two control groups but was less effective than OVA+522GGNP. To determine the activation of Ag-specific cytotoxic CD8 T lymphocytes that can eradicate tumor cells [23,24], we first quantitated the number of the $OVA_{257-264}$-specific CD44^{high} CD8 T cells [25] to determine expansion. OVA+522GGNP immunization increased the number of CD44^{high} CD8 T cells by 4- and 2.5- fold compared to untreated and OVA only-treated mice, respectively **(Figure 6B)**. Moreover, $OVA_{257-264}$-specific IFN-ɣ$^{+}$ CD8 T cells also increased 3- and 2.5- fold when mice were immunized with OVA+522GGNP compared to untreated and OVA only group, respectively **(Figure 6C)**. Consistent with our previous study [7], OVA+522NP immunization increased $OVA_{257-264}$-specific CD8 T cell responses compared to controls; however, OVA+522GGNP immunization induced stronger T cell responses than OVA+522NP immunization. which could be because of augmented DC activity triggered by 522GGNP.

(A) (B) (C)

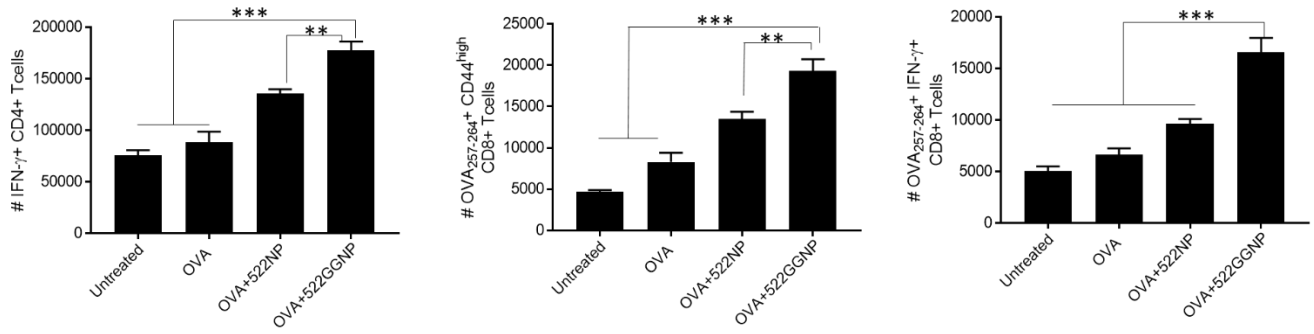

Figure 6. ***In vivo*** **T cell activation**

Following immunization, spleens were collected and analyzed by flow cytometry. **(A)** Number of IFN-γ^+ CD4 T ($CD3^-CD4^+$) cells; **(B)** Number of $OVA_{257-264}$-specific $CD44^{high}$ CD8 T ($CD3^-CD8^+$) cells; **(C)** Number of $OVA_{257-264}$-specific IFN-γ^+ CD8 T cells. Results are reported as mean ± SEM, $^{**}p<0.01$, $^{***}p<0.001$, n=4, one-way ANOVA.

In vivo **NK cell assay**

CD70 is a co-stimulatory molecule expressed on DCs that interacts with CD27 on NK cells and induces NK cell activation [26]. As seen in **Figure 7A**, both 522NPs and 522GGNPs induced upregulation of CD70 on DCs. We then investigated NK cell activation *in vivo*. Frequency of both $CD69^{high}$ and IFN-γ^+ NK cells increased 2.5-fold compared the untreated group **(Figure 7B,C)**. Consistent with the results of the T cell activation studies, 522NP immunization also induced NK cell activation, but the extent was less than that with 522GGNP immunization. Combined with results of the T cell activation study, these results suggest that 522GGNP immunization is effective in expanding cytotoxic cells that can kill malignant tumor cells.

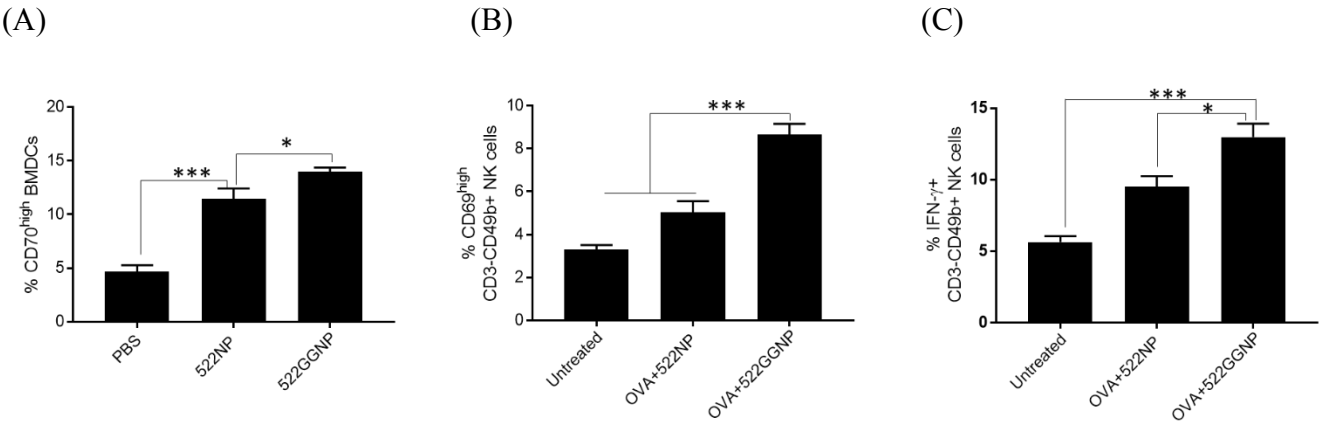

Figure 7. ***In vivo*** **NK cell activation**

(A) Expression of CD70 on BMDCs was measured by flow cytometry. Results are reported as mean ± SD, *p<0.05, ***p<0.001, n=3, one-way ANOVA. **(B,C)** Spleens of immunized mice were harvested and analyzed by flow cytometry. **(B)** Number of $CD69^{high}$ NK ($CD3^{-}CD49b^{+}$) cells. **(C)** Number of IFN-γ^{+} NK cells. Results are reported as mean ± SEM, *p<0.05, ***p<0.001, n=4, one-way ANOVA.

Tumor challenge

In vivo therapeutic efficacy of OVA+522GGNP immunization was evaluated in a murine melanoma tumor model. B16F10-OVA tumors became palpable on d 11 after tumor cell injection and mice were immunized by once daily dosing of the vaccine formulation from d 11 to d 15. Both untreated and OVA alone treated groups showed rapid tumor growth, where all of the mice had tumors ≥1500 mm^3 by d 22 and d 24, respectively **(Figure 8)**. Consistent with our previous study [7], OVA+522NP immunization was effective in inhibiting tumor growth ($p<0.001$). However, OVA+522GGNP immunization showed enhanced therapeutic efficacy compared to OVA+522NP vaccination ($p<0.001$). Average tumor volume of OVA+522NP and

OVA+522GGNP immunized animals on d 24 was 729 mm^3 and 339 mm^3, respectively. To further examine the therapeutic outcome of 522GGNP treatment, we performed survival analysis **(Figure 8B)**. OVA+522GGNP immunized animals showed significantly enhanced survival ($p<0.01$) compared to other treatments, which further demonstrates the anti-tumor efficacy of 522GGNP treatment.

(A)

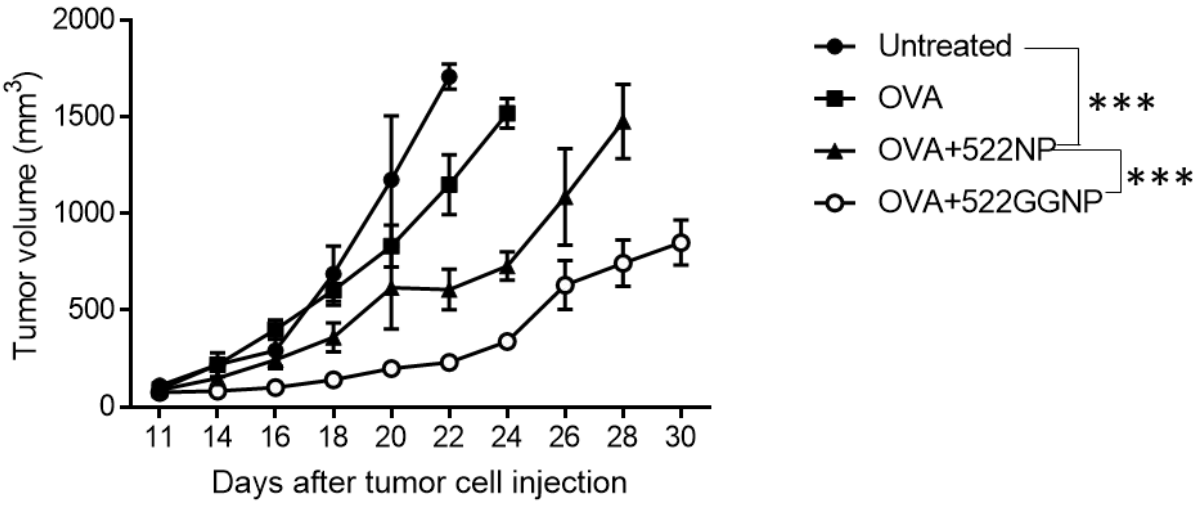

(B)

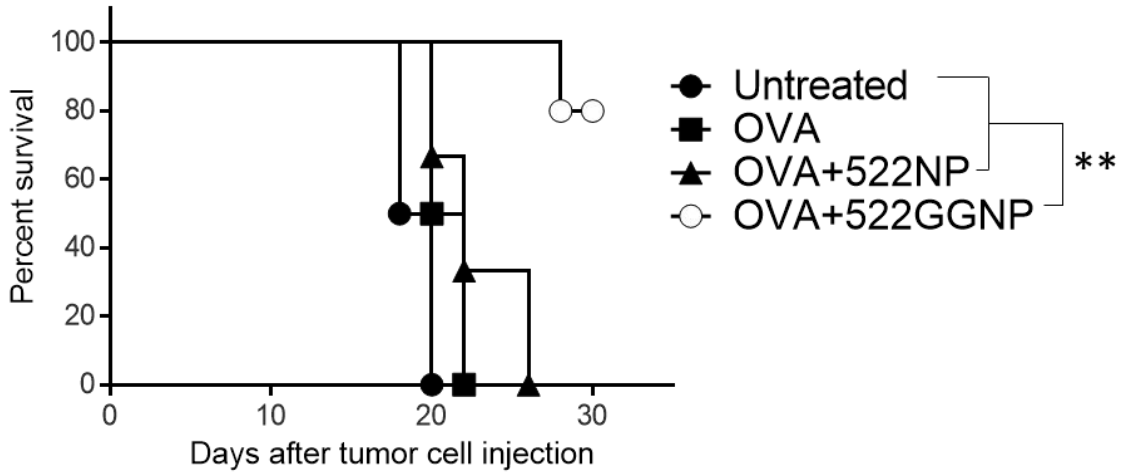

Figure 8. Tumor challenge using B16F10-OVA melanoma tumor model

C57BL/6 mice with established B16F10-OVA tumors were randomized and vaccine doses were administered over five days (d 11-15). **(A)** Tumor growth curves. Results are reported as mean ± SEM, ***p<0.001, n=4~5, Two-way ANOVA with *post hoc* Tukey's test. **(B)** Survival data for various treatments. **p<0.01, Log-rank (Mantel–Cox) test.

Discussion

Nanoparticulate delivery of TLR7/8 agonists can extend their application in cancer immunotherapy. Currently, TLR7/8 agonists are limited to topical administration (ClinicalTrials.gov; NCT01808950, NCT01676831) and intratumoral injection (NCT02556463). In the studies where TLR7/8 agonists have been utilized as the vaccine adjuvant, peptides derived from tumor-associated Ag (TAA) were administered S.C. (NCT01748747, NCT00960752) and the TLR7/8 agonists were applied topically on the tumor. However, co-delivery of antigen and adjuvant to the same Ag-presenting cells is critical for eliciting Ag-specific T cell response [27,28]. Previous studies show that co-encapsulation of antigen and TLR

agonist potentiates strong humoral immunity, which further demonstrates the importance of co-delivery of antigen and adjuvant[29,30]. Therefore, a formulation that can deliver TLR7/8 agonists via S.C. or I.M. injection[31] together with TAA-peptides is needed.

We investigated PLGA NPs for TLR7/8 agonist delivery because of the excellent biocompatibility and safety profile of PLGA [14]. PLGA is non-immunogenic, and degrades to lactic acid and glycolc acid , both which can be further eliminated through endogenous metabolic pathways. In our study, we observed that blank PLGA nanoparticles without drug encapsulation (BlankNPs) do not activate TLR 7 and 8 reporter cells **(Supplement figure 1)**. Additionally, treatment with BlankNPs did not promote *in vivo* T cell activation **(Supplement figure 2)**, which further supports that PLGA NP do not have immunologic activity. We utilized PLGA with PLA:PGA molar ratio of 50:50 with intermediate MW (inherent viscosity=0.55~0.75 dl/g), as NPs fabricated with the specific PLGA have been shown to provide consistent size, surface charge, and release kinetics [32,33]. Size of NPs was fine-tuned to 200 nm, as NPs ≤300 nm have been reported to efficiently internalize into DCs and can trigger enhanced T cell response and humoral immunity compared to larger nanoparticles and microparticles[34,35]. Additionally, NPs with size of 100 ~ 200 nm can directly enter lymphatic system via lymphatic capillaries within hours after injection[36].

Low drug loading was an issue in our previous study (~1 μg/mg of NPs) [7]. Low encapsulation of imidazoquinoline derivatives in PLGA nanoparticles has been reported previously [37,38]. 522 is a moderately hydrophobic compound (logP = 2.74). However, it has increased solubility in 2.5 % PVA solution (30 μg/ml). Thus, 522 can diffuse out from the oil phase to aqueous phase during the fabrication process, which could lead to low encapsulation efficacy. In the present study, encapsulation efficiency increased several fold in 522GGNP

compared to our previous 522NP. We presume the increased encapsulation of 522 in 522GGNP was because of two reasons. First, the double-emulsion evaporation method can result in higher encapsulation efficiency for both hydrophilic and hydrophobic drugs [39]. Second, the presence of the bicarbonate salt in the primary aqueous phase could also have affected the drug loading. The use of 1% PVA without sodium bicarbonate as the primary phase resulted in only 6% encapsulation efficacy **(Supplement table 1)**. We also tested 1% PVA solutions containing sodium chloride or sodium phosphate, as the addition of salt in primary emulsion can stabilize the emulsion [40]. In our hands, these salt solutions failed to form a stable emulsion with 522 and resulted in 5% and 7% encapsulation efficiencies, respectively. In addition to their low encapsulation efficiency, these nanoparticles also had larger size.

The presence of sodium bicarbonate also contributed to the acidic pH-response release kinetics of 522GGNPs. Utilizing the bicarbonates to introduce pH-sensitive drug release has been previously reported [41,42]. In acidic pH, bicarbonates react with H^+ to form carbonic acid, which dissociates to release CO_2 gas that can mechanically disrupt the polymer shell and facilitate the rapid release of the drug payload. Ultrasound imaging confirmed acidic pH-dependent gas-generation by 522GGNPs but not 522NPs, which supports the proposed mechanism of drug release. Additionally, 522 can be protonated (N3 position) in acidic pH **(Supplement figure 3)**, resulting in improved aqueous solubility and rapid release from NPs. Acidic-pH responsive release can be important for effective DC activation by TLR7/8 agonists. Both TLR7 and 8 are located on the luminal side of endo-lysosomes, which are acidic cellular compartments (pH 4~6) [16]. From flow cytometry and confocal data, we confirmed that 522GGNPs localize to endo/lysosome. Based on these results, we expect 522GGNPs can improve the delivery of 522 to the endo-lysosomes [6,41]. Compared to the conventional 522NPs,

522GGNPs resulted in a much stronger DC activation, further substantiating improved 522 delivery to the target site. In addition to upregulation of co-stimulatory molecules, 522GGNP significantly enhanced the antigen presentation via MHC I.

T cells are key players in cancer immunotherapy because of their ability to directly kill the tumor cells and activate other immune cells [23,24]. In this study, we found 522GGNP immunization increased the number of IFN-ɣ$^+$ CD4 T cells, which can activate CD8 T cells and NK cells [22,43]. This data implies 522GGNP immunization can potentiate a Th1 response [44]. As CD4 T cells are primarily activated via CD40-CD40L signaling [45], it is likely 522GGNPs' ability to increase CD40 expression on DCs enables the expansion of effector CD4 T cells. In addition, increased expression of MHC II on 522GGNP treated DCs further suggests 522GGNP is effective in activating effector CD4 T cells [46]. 522GGNP immunization also increased the number of Ag-specific effector CD8 T cells. Consistent with our previous study [7], OVA+522NP increased both $OVA_{257-264}$-specific CD44^{high} CD8 T cells and $OVA_{257-264}$-specific IFN-ɣ$^+$ CD8 T cells compared to OVA only, which demonstrates the potent adjuvanticity of polymeric nanoparticles encapsulating TLR7/8 agonists. The greater $OVA_{257-264}$-specific CD8 T cell expansion observed with 522GGNP immunization compared to that with 522NP was likely the result of enhanced Ag-presentation and co-stimulatory molecule signaling by DCs that primed CD8 T cells and further potentiated by IFN-ɣ$^+$ CD4 T cells.

NK cells also play major role in cancer immunotherapy as they can secrete IFN-ɣ upon activation and directly kill the tumor cells with cytotoxic granules [47]. As NK cells can be activated by DC-NK cell interaction and IFN-ɣ secreted by T cells [48], we investigated NK cell expansion following 522GGNP immunization. Similar to the observed increase in T cell activation, 522GGNP immunization increased both CD69^{high} NK cells and IFN-ɣ$^+$ NK cells.

CD69 expression triggers cytolytic activation of NK cells [49]. Activation of NK cells can provide several benefits in cancer immunotherapy. First, NK cells can kill the tumor cells before CD8 T cells are primed by DCs. It has been reported that 7-9 days are required to generate antigen-specific CD8 T cells after immunization, but the tumor cells continue to proliferate during that time span [50]. However, NK cells become effective as early as few hours after immunization, and kill the tumor cells before CD8 T cells are primed [51]. This leads to another benefit of activated NK cells, as NK cells can induce immunogenic tumor cell death [52,53]. As a result, more TAAs will be available to DCs. In addition, IFN-ɣ secretion by NK cells can modulate other Ag presenting cells and T cells for Th1 response [54].

To evaluate whether enhanced antigen-specific CD8 T cell and NK cell response by OVA+522GGNP immunization could lead to improved anticancer efficacy, we performed a tumor challenge study using B16F10-OVA tumor model. While OVA+522NP immunization was effective in inhibiting tumor growth compared to untreated and OVA only treatment, OVA+522GGNP immunization showed superior therapeutic efficacy. Interestingly, OVA+522GGNP showed effectiveness two days earlier (d 16) than OVA+522NP (d 18). As 7~10 days are required to prime CD8 T cells, it is possible that activated NK cells could have contributed to the early effectiveness of OVA+522GGNP treatment. Taken together, our data thus demonstrate 522GGNP can elicit robust antigen-specific CD8 T cell and NK cell responses, resulting in enhanced therapeutic efficacy compared to that with 522NP.

Peptide/protein based TAAs including cancer-testis antigens (MAGE-1, NY-ESO-1) [55] , melanoma antigens (gp100, MART-1) [56], and prostate cancer antigens (PSA, PSP) [57], have been evaluated in combination with TLR agonists as cancer vaccines in the clinic. In this study, we utilized OVA as a model antigen to demonstrate the potency of 522GGNP as an adjuvant

platform for protein antigens. Further, we chose to co-inject the antigen and agonist loaded nanoparticles rather than co-encapsulate the antigen with the agonist in nanoparticles to independently test the effectiveness of acid responsive nanoparticles. In addition to encapsulating small molecules, we expect that GGNP can be utilized to co-encapsulate peptide/protein antigens. Previous studies report that encapsulation of tumor cell lysate in polymeric NPs enhances immunogenicity of cancer vaccine[58,59]. Future studies will examine the effectiveness of co-encapsulating TLR 7/8 agonists with specific tumor antigens.

Conclusion

In this study, we introduced the use of an acidic pH responsive NP formulation for endo/lysosomal delivery of TLR7/8 agonists. The new formulation was characterized by higher drug encapsulation and acidic-pH responsive release kinetics. 522GGNPs showed more potent NK cell and CD8 T cell responses than 522NPs. Our results suggest acidic-pH responsive, gas-generating nanoparticles is an efficient drug delivery platform for TLR7/8 agonists for cancer immunotherapy.

Conflicts of interest

D.M.F has patent on 522. All authors declare that they have no other conflict of interest.

Acknowledgments

We thank Guillermo Marques in the University Imaging Center (University of Minnesota) for ultrasound imaging training and Elizabeth Lundstrom in the Geochemical lab (University of

Minnesota) for ICP-EOS analysis. We also thank Han Seung Lee in the Characterization Facility (University of Minnesota), which receives partial support from NSF through the MRSEC program (The Hitachi SU8320 cryoSEM and cryospecimen preparation system were provided by NSF MRI DMR-1229263), for the Cryo-TEM imaging.

This work was supported by the Grant in aid program, University of Minnesota (to J.P.), GAP award (to J.P.), Masonic Cancer Center, University of Minnesota (to T.S.G.), the Prostate and Urological Cancer Translational Working Group (to T.S.G.), and the Randy Shaver Cancer Research & Community Fund (to T.S.G., D.M.F.)

Data Availability

The raw/processed data required to reproduce these findings cannot be shared at this time as the data also forms part of an ongoing study.

References

1 R. D. Weeratna, S. R. Makinen, M. J. McCluskie and H. L. Davis, *Vaccine*, 2005, **23**, 5263–5270.

2 K. Kastenmüller, U. Wille-Reece, R. W. B. Lindsay, L. R. Trager, P. A. Darrah, B. J. Flynn, M. R. Becker, M. C. Udey, B. E. Clausen, B. Z. Igyarto, D. H. Kaplan, W. Kastenmüller, R. N. Germain and R. A. Seder, *J. Clin. Invest.*, 2011, **121**, 1782–1796.

3 Y. Kawarada, R. Ganss, N. Garbi, T. Sacher, B. Arnold and G. J. Hammerling, *J. Immunol.*, 2001, **167**, 5247–5253.

4 M. F. Bachmann and G. T. Jennings, *Nat. Rev. Immunol.*, 2010, **10**, 787–96.

5 G. M. Lynn, R. Laga, P. A. Darrah, A. S. Ishizuka, A. J. Balaci, A. E. Dulcey, M. Pechar, R. Pola, M. Y. Gerner, A. Yamamoto, C. R. Buechler, K. M. Quinn, M. G. Smelkinson, O. Vanek, R. Cawood, T. Hills, O. Vasalatiy, K. Kastenmüller, J. R. Francica, L. Stutts, J. K. Tom, K. A. Ryu, A. P. Esser-Kahn, T. Etrych, K. D. Fisher, L. W. Seymour and R. A. Seder, *Nat. Biotechnol.*, 2015, **33**, 1201–1210.

6 S. Akira and K. Takeda, *Nat. Rev. Immunol.*, 2004, **4**, 499–511.

7 H. Kim, L. Niu, P. Larson, T. A. Kucaba, K. A. Murphy, B. R. James, D. M. Ferguson, T. S. Griffith and J. Panyam, *Biomaterials*, 2018, **164**, 38–53.

8 C. E. Schiaffo, C. Shi, Z. Xiong, M. Olin, J. R. Ohlfest, C. C. Aldrich and D. M. Ferguson, *J. Med. Chem.*, 2014, **57**, 339–347.

9 P. Larson, T. A. Kucaba, Z. Xiong, M. Olin, T. S. Griffith and D. M. Ferguson, *ACS Med. Chem. Lett.*, 2017, **8**, 1148–1152.

10 N. Grabowski, H. Hillaireau, J. Vergnaud, N. Tsapis, M. Pallardy, S. Kerdine-Römer and E. Fattal, *Int. J. Pharm.*, 2015, **482**, 75–83.

11 B. R. James, E. L. Brincks, T. A. Kucaba, L. Boon and T. S. Griffith, *Cancer Immunol. Immunother.*, 2014, **63**, 685–697.

12 C. J. Ke, W. L. Chiang, Z. X. Liao, H. L. Chen, P. S. Lai, J. S. Sun and H. W. Sung, *Biomaterials*, 2013, **34**, 1–10.

13 J. Panyam, S. K. Sahoo, S. Prabha, T. Bargar and V. Labhasetwar, *Int. J. Pharm.*, 2003, **262**, 1–11.

14 J. Panyam and V. Labhasetwar, *Adv. Drug Deliv. Rev.*, 2003, **55**, 329–347.

15 M. a Dobrovolskaia, P. Aggarwal, J. B. Hall and S. E. Mcneil, *Mol. Pharm.*, 2009, **5**, 487–495.

16 R. J. Ulevitch, *Nat. Rev. Immunol.*, 2004, **4**, 512–20.

17 C. B. Thompson, T. Lindsten, J. A. Ledbetter, S. L. Kunkel, H. A. Young, S. G. Emerson, J. M. Leiden and C. H. June, *Proc. Natl. Acad. Sci.*, 1989, **86**, 1333–1337.

18 P. Guermonprez, J. Valladeau, L. Zitvogel, C. Théry and S. Amigorena, *Annu. Rev. Immunol.*, 2002, **20**, 621–667.

19 D. Dudziak, A. Kampfhorst, G. Heidkamp, V. Buhcholz, C. Trumpfheller, S. Yamazaki, C. Cheong, K. Liu and H. Lee, *Science (80-.).*, 2007, **315**, 107–112.

20 J. M. Schenkel, K. A. Fraser, V. Vezys and D. Masopust, *Nat. Immunol.*, 2013, **14**, 509–513.

21 S. E. Macatonia, N. A. Hosken, M. Litton, P. Vieira, C. S. Hsieh, J. A. Culpepper, M. Wysocka, G. Trinchieri, K. M. Murphy and A. O'Garra, *J. Immunol.* , 1995, **154**, 5071–5079.

22 D. J. Shedlock, *Science (80-.).*, 2003, **300**, 337–339.

23 C. A. Klebanoff, L. Gattinoni, P. Torabi-Parizi, K. Kerstann, A. R. Cardones, S. E. Finkelstein, D. C. Palmer, P. A. Antony, S. T. Hwang, S. A. Rosenberg, T. A. Waldmann and N. P. Restifo, *Proc. Natl. Acad. Sci.*, 2005, **102**, 9571–9576.

24 C. A. Klebanoff, L. Gattinoni and N. P. Restifo, *Immunol. Rev.*, 2006, **211**, 214–224.

25 S. Huet, H. Groux, B. Caillou, H. Valentin, A. M. Prieur, S. Huet, H. Groux, H. Valentin, M. Prieur and A. Bernard, *J. Immunol.*, 1989, **143**, 798–801.

26 F. C. Yang, K. Agematsu, T. Nakazawa, T. Mori, S. Ito, T. Kobata, C. Morimoto and A. Komiyama, *Immunology*, 1996, **88**, 289–293.

27 X. Q. Zhang, C. E. Dahle, G. J. Weiner and A. K. Salem, *J. Pharm. Sci.*, 2007, **96**, 3283–3292.

28 X. Q. Zhang, C. E. Dahle, N. K. Baman, N. Rich, G. J. Weiner and A. K. Salem, *J. Immunother.*, 2007, **30**, 469–478.

29 Y. Tao, Y. Zhang, E. Ju, H. Ren and J. Ren, *Nanoscale*, 2015, **7**, 12419–12426.

30 V. B. Joshi, A. Adamcakova-Dodd, X. Jing, A. Wongrakpanich, K. N. Gibson-Corley, P. S. Thorne and A. K. Salem, *AAPS J.*, 2014, **16**, 975–985.

31 C. Pegoraro, S. MacNeil and G. Battaglia, *Nanoscale*, 2012, **4**, 1881–1894.

32 A. R. Kirtane, H. L. Wong, B. R. Guru, L. G. Lis, G. I. Georg, V. J. Gurvich and J. Panyam, *Mol. Pharm.*, 2015, **12**, 2912–2923.

33 L. Niu and J. Panyam, *J. Control. Release*, 2017, **248**, 125–132.

34 S. Heidegger, D. Gößl, A. Schmidt, S. Niedermayer, C. Argyo, S. Endres, T. Bein and C. Bourquin, *Nanoscale*, 2016, **8**, 938–948.

35 V. B. Joshi, S. M. Geary and A. K. Salem, *AAPS J.*, 2013, **15**, 85–94.

36 V. Manolova, A. Flace, M. Bauer, K. Schwarz, P. Saudan and M. F. Bachmann, *Eur. J. Immunol.*, 2008, **38**, 1404–1413.

37 M. B. Heo and Y. T. Lim, *Biomaterials*, 2014, **35**, 590–600.

38 C. Primard, J. Poecheim, S. Heuking, E. Sublet, F. Esmaeili and G. Borchard, *Mol. Pharm.*, 2013, **10**, 2996–3004.

39 M. Iqbal, N. Zafar, H. Fessi and A. Elaissari, *Int. J. Pharm.*, 2015, **496**, 173–190.

40 K. F. Pistel, T. Kissel, *J. Microencapsul.*, 2000, **17**, 467–483.

41 Q. Liu, X. Chen, J. Jia, W. Zhang, T. Yang, L. Wang and G. Ma, *ACS Nano*, 2015, **9**, 4925–4938.

42 C. J. Ke, T. Y. Su, H. L. Chen, H. L. Liu, W. L. Chiang, P. C. Chu, Y. Xia and H. W. Sung, *Angew. Chemie - Int. Ed.*, 2011, **50**, 8086–8089.

43 S. Jost, P. J. Tomezsko, K. Rands, I. Toth, M. Lichterfeld, R. T. Gandhi and M. Altfeld, *J. Virol.*, 2014, **88**, 8349–8354.

44 S. J. Szabo, B. M. Sullivan, C. Stemmann, A. R. Satoskar, B. P. Sleckman and L. H. Glimcher, *Science (80-.).*, 2002, **295**, 338–343.

45 S. P. Schoenberger, R. E. M. Toes, E. I. H. Van der Voort, R. Offringa and C. J. M. Melief, *Nature*, 1998, **393**, 480–483.

46 D. L. Farber, M. Luqman, O. Acute and K. Bottomly, *Cell*, 1995, **2**, 249–259.

47 C. H. M. J. Van Elssen, T. Oth, W. T. V Germeraad, G. M. J. Bos and J. Vanderlocht, *Clin. Cancer Res.*, 2014, **20**, 1095–1103.

48 M. A. Degli-Esposti and M. J. Smyth, *Nat. Rev. Immunol.*, 2005, **5**, 112–124.

49 F. Borrego, M. J. Robertson, J. Ritz, J. Peña and R. Solana, *Immunology*, 1999, **97**, 159–165.

50 S. Jung, D. Unutmaz, P. Wong, G. I. Sano, K. De Los Santos, T. Sparwasser, S. Wu, S. Vuthoori, K. Ko, F. Zavala, E. G. Pamer, D. R. Littman and R. A. Lang, *Immunity*, 2002, **17**, 211–220.

51 N.-L. L. Pham, L. L. Pewe, C. J. Fleenor, R. A. Langlois, K. L. Legge, V. P. Badovinac and J. T. Harty, *Proc. Natl. Acad. Sci.*, 2010, **107**, 12198–12203.

52 G. Kroemer, L. Galluzzi, O. Kepp and L. Zitvogel, *Annu. Rev. Immunol.*, 2013, **31**, 51–72.

53 L. Aymeric, L. Apetoh, F. Ghiringhelli, A. Tesniere, I. Martins, G. Kroemer, M. J. Smyth and L. Zitvogel, *Cancer Res.*, 2010, **70**, 855–858.

54 A. Martín-Fontecha, L. L. Thomsen, S. Brett, C. Gerard, M. Lipp, A. Lanzavecchia and F. Sallusto, *Nat. Immunol.*, 2004, **5**, 1260–1265.

55 M. Scanlan, A. Gure, A. Jungbluth and L. Old, *Immunol. Rev.*, 2002, **188**, 22–32.

56 T. J. De Vries, A. Fourkour, T. Wobbes, G. Verkroost, D. J. Ruiter and G. N. P. Van Muijen, *Cancer Res.*, 1997, 3223–3230.

57 J. Dannull, P. A. Diener, L. Prikler, G. Furstenberger, T. Cerny, U. Schmid, D. K. Ackermann and M. Groettrup, *Cancer Res.*, 2000, **60**, 5522–5528.

58 G.-N. Shi, C.-N. Zhang, R. Xu, J.-F. Niu, H.-J. Song, X.-Y. Zhang, W.-W. Wang, Y.-M. Wang, C. Li, X.-Q. Wei and D.-L. Kong, *Biomaterials*, 2017, **113**, 191–202.

59 B. P. Gross, A. Wongrakpanich, M. B. Francis, A. K. Salem and L. A. Norian, *AAPS J.*, 2014, **16**, 1194–1203.

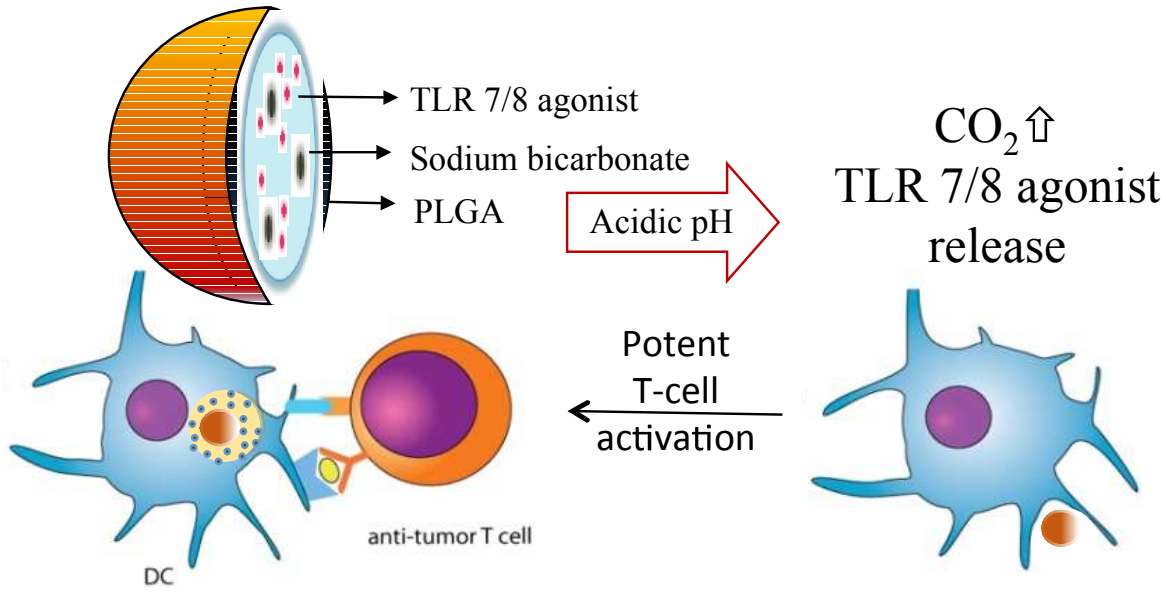

Acidic-pH responsive PLGA NPs enhance endo/lysosomal delivery of TLR7/8 agonist and elicit stronger anti-tumor T cell response than conventional PLGA NPs